NUMERICAL ASSESSMENT OF AN EXPERIMENTAL PROCEDURE APPLIED TO DCB TESTS

Nagore Insausti[1], Itziar Adarraga[1], Juan De Gracia[1], Ainhoa Arrese[1], Faustino Mujika[1]

[1]Materials + Technologies Group / Mechanics of Materials, Department of Mechanical

Engineering, Faculty of Engineering of Gipuzkoa, University of the Basque Country UPV/EHU

Plaza Europa, 1, 20018 Donostia-San Sebastián, Spain.

E-mail: nagore.insausti@ehu.eus

Abstract

Numerical analysis of the analytic model of an experimental procedure to determine the crack length, the compliance and the energy release rate has been developed. As a first step, bending tests at different spans have been numerically simulated with the purpose of obtaining the flexural and out-of-plane shear moduli of the material. Then the crack length has been determined from the numerical compliance, considering the material properties previously obtained. The critical energy release rate has also been determined analytically and numerically. There is agreement between the numerical results and those obtained from the analytic model of the experimental procedure.

Key words: Delamination; Double Cantilever Beam; Crack length; Energy release rate; Polymer matrix composites

---

Nomenclature	
a, Δa	crack length and crack increment, respectively
A	cross sectional area
A_R, B_R, C_R	third order regression coefficients
b	beam or specimen width
C, C_{num}, C_{sys}	specimen, numerical and system compliance, respectively

E_1, E_2, E_3	longitudinal, in-plane and out-of-plane elastic moduli, respectively
E_f	flexural modulus
G_{12}	in-plane shear modulus
G_{13}, G_{23}	out-of-plane shear moduli
G_I, G_{Ic}	strain energy release rate and critical fracture toughness, respectively
h	beam thickness or thickness of the cracked arm
I	second moment of area
k	spring constant
L	beam length
m	slope of the load-displacement curve
M, Q	bending moment and shear force, respectively
P	applied load
q_{10}, q_{30}	distributed forces of the linear elastic foundation
U, U^*	strain energy and complementary strain energy, respectively
x_1, x_2, x_3	parameters of the linear elastic foundation
$\beta_1, \beta_2, \beta_3, \beta_4$	x_1, x_2 and x_3 dependent parameters
δ, δ_3	beam displacement and crack tip beam displacement, respectively
θ_3	crack tip beam bending angle
v_{12}, v_{13}, v_{23}	Poisson's ratios

1. Introduction

Carbon Fibre Reinforced Polymer composites (CFRP) are interesting due to the combination of being lightweight and having high specific strength. Nevertheless, when interlaminar cracks appear their stiffness and strength may be significantly reduced. Delamination is considered as the most frequent damage mechanism in laminated composites. Thus, the study of interlaminar fracture toughness is one of the main aspects in CFRP. The Double Cantilever Beam (DCB) test is widely used in order to determine interlaminar failure in laminated composites. The DCB test has been standardized for CFRP [1,2].

As a first approach, each arm was considered as a cantilever beam in pure bending, fixed at the crack tip. It is evident that this is not the actual case, because the beam ahead of the delamination front is not infinitely stiff and therefore, the beam will have a shear deformation and a root rotation. The approach was improved assuming that the interaction between both arms could be considered as an elastic foundation. The effect of root flexibility was first studied by Kanninen [3,4], who proposed an improved beam model for isotropic DCB specimens. Whitney [5] and Williams [6] extended the analysis to orthotropic material.

In the DCB standards [1,2] an equivalent crack length is defined in order to include the non null rotation at the crack tip. Thus, the crack length optically determined at the specimen edge is corrected, obtaining a greater crack length. Different data reduction methods for achieving the critical energy release rate were compared by Hashemi et al. [7]. This research concluded the necessity of correcting the crack length in the methods based on the beam theory, since the beam is not perfectly clamped. This correction of the crack length based on a compliance calibration method was named Corrected Beam Theory (CBT). The case of great displacements was considered including a linear springs' elastic foundation [8].

Olsson [9] proposed to compute the overall compliance based on classical beam theory corrected for shear deformation and taking into account transverse compliance in the un-cracked part and the Saint Venant effects ahead of the crack front. In this work the analytic results were compared with those obtained by means of the Finite Element Method (FEM). More analytical and experimental analyses have been carried out [10-23] and a comparative analysis of the different elastic foundation models can be found in [24].

The Virtual Crack Closure Technique (VCCT) and the Cohesive Zone Model (CZM) are among the most widely used methods for the research of interlaminar fracture

toughness via FEM. VCCT was introduced by Rybicki and Kanninen [25] and is efficient to determine the energy release rate [26-36]. CZM is mainly used for analysing crack propagation [37-44].

Recently, Huang et al. have provided an analytical expression for an elastic-plastic bilinear cohesive law of DCB specimens [45] and a research taking into account the finite length of DCB specimens has also been developed [46]. Xu and Guo have proposed a double compliances method [47]. The first compliance is achieved from the initial slope of the load-displacement curve and the second from the unloading test. These compliances are linked to the initial and final measures of the crack length, respectively. These values are substituted into the compliance equation and, therefore, an expression to determine the crack length is obtained. Consequently, the energy release rate can also be calculated.

A method for obtaining the interlaminar fracture toughness of DCB specimens without optically measuring the crack length has been introduced recently by De Gracia et al. [48]. They proposed a linear elastic foundation with three linear parts. The initial linear parts are adopted based on their similitude to the solutions of linear elastic foundations. In that approach it is shown that the distances where compressive stresses act depend on material properties and that the distance where tensile stresses act depends on the previous ones and on the thickness of the specimen.

On the basis of that model, an experimental procedure to determine the crack length based on the compliance of the specimen has been proposed. In that way, the determined crack length includes all the sources of change of the compliance. It is worth noting that the experimental procedure also proposes the way to discount the compliance of the system. Having determined the crack length for each pair of experimental values of load and displacement given by the testing machine, the energy release rate is determined point by point, obtaining the R-curve of the test.

The aim of the present work is to carry out a virtual test, including the determination of the out-of-plane shear modulus and the flexural modulus by the same procedure that is used experimentally. This procedure is based on [49] and includes the effects of flexural, shear and local effects. The three characteristic parameters are obtained by performing three-point bending tests at different spans. In order to validate numerically the experimental procedure proposed in [48] the crack length is determined based on the compliance of the system and adopting the previously calculated values of the flexural and out-of-plane shear moduli in the FEM analysis. Furthermore, the strain energy release rate G_I has been determined via FEM by different methods. Finally, results obtained from virtual tests are compared with those achieved from the analytic based data reduction method.

2. Analytical basis of the experimental procedure

2.1. DCB tests and specimens

The DCB test configuration shown in Fig. 1 is the most popular method used to evaluate mode I interlaminar fracture toughness. In this test a pre-cracked specimen is loaded at one edge with loading blocks or piano hinges. The standardized procedure requires the measurement of the delamination length a, as the load is applied. The main drawback of this procedure is the requirement of measuring the crack length during the test.
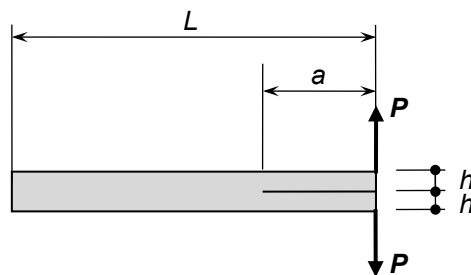

Fig. 1. Configuration of the DCB specimen.

A method to determine the crack length based on the compliance of the specimen has been proposed recently [48]. The basis of this analytical approach is a simplified model of the stress distribution on the un-cracked part of the specimen as shown in Fig. 2. Once the elastic properties relative to the specimen have been obtained, the crack length is determined without optical measurements, based on the compliance.
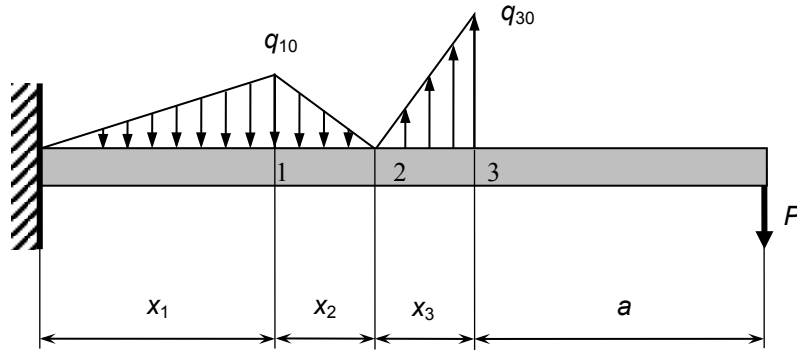

Fig. 2. Distributed force along the beam.

Applying Engesser-Castigliano's theorem [48,51,52], the displacement of the half of the specimen at the loading point can be determined as follows:

$$\delta = \delta_3 + \theta_3 a + \frac{Pa^3}{3E_f I} + \frac{6Pa}{5G_{13}A} \tag{1}$$

Being P the applied load at the end point, a the length of the crack, E_f the flexural modulus, G_{13} the out-of-plane shear modulus, I the second moment of area, A the cross sectional area, δ_3 the displacement at the crack tip and θ_3 the bending angle at the crack tip. Those two last terms are:

$$\delta_3 = \frac{hP}{E_3 b}(\beta_4 + \beta_2 a) \qquad \theta_3 = \frac{P}{12E_f I}(\beta_3 + 3\beta_1 a) \tag{2}$$

Being E_3 the out-of-plane Young's modulus, b the width of the specimen and h the thickness of each arm. The parameters β are dependent only on the distances x_1, x_2 and x_3 that were determined in [48]:

6

$$\beta_1 = \frac{x_1^2 + 3x_1x_2 + 4x_1x_3 + 3x_2^2 + 8x_2x_3 + 5x_3^2}{x_1 + 2x_2 + 2x_3}$$

$$\beta_2 = \frac{3}{x_3\left(x_1 + 2x_2 + 2x_3\right)}$$

$$\beta_3 = \frac{x_1^2x_3 + 3x_1x_3^2 + 3x_1x_2x_3 + 3x_2^2x_3 + 6x_2x_3^2 + 3x_3^3}{x_1 + 2x_2 + 2x_3}$$

$$\beta_4 = \frac{x_1 + 2x_2 + 3x_3}{x_3\left(x_1 + 2x_2 + 2x_3\right)}$$

(3)

Taking into account Eq. (1) and that the compliance is the ratio of opening displacement of the crack mouth 2δ to the applied load P at the end point, the compliance of the DCB specimen can be determined from the following expression:

$$C = \frac{2\delta}{P} = \frac{2a^3}{3E_fI} + \frac{2\beta_1a^2}{4E_fI} + 2\left(\frac{6}{5G_{13}A} + \frac{\beta_2h}{bE_3} + \frac{\beta_3}{12E_fI}\right)a + \frac{2\beta_4h}{bE_3}$$

(4)

In experimental practice, if the displacement given by the testing machine is used, it is necessary to apply the correction related to the system compliance [48].

The strain energy release rate G_I, which is a measure of fracture toughness, is obtained differentiating the compliance with respect to the crack length [53]. Considering linear elastic behaviour:

$$G_I = \frac{P^2}{2b}\frac{\partial C}{\partial a}$$

(5)

Replacing Eq. (4) in Eq. (5), G_I can be expressed as follows:

$$G_I = \frac{P^2a^2}{bE_fI} + \frac{\beta_1P^2a}{2bE_fI} + \frac{6P^2}{5b^2hG_{13}} + \frac{\beta_2hP^2}{b^2E_3} + \frac{\beta_3P^2}{12bE_fI}$$

(6)

Since the objective is to determine the crack length by means of Eq. (4), it is necessary to have the values of the flexural and out-of-plane shear moduli. These are calculated following the experimental procedure using FEM, as it is explained in the next section.

2.2. Determination of E_f and G_{13}

In experimental practice, previous to a DCB test, bending tests are performed in order to determine the flexural and the out-of-plane shear moduli of the material. Mujika [49]

7

proposed a procedure to determine the flexural modulus and shear modulus by performing three-point bending tests at different spans. The experimental displacement given by the testing machine was used and therefore local deformation effects were taken into account. Those effects include the deformation of the specimen in the thickness and the inherent deformability of components of the test setup.

In this work three-point bending tests are simulated via FEM and a similar procedure to that described in [49] is followed in order to obtain the flexural and out-of-plane shear moduli. The equations differ because in this approach the support rollers have not been considered and half of the beam is analysed due to symmetry. The reaction point is approached by a linear spring in order to take into account local deformations. Indeed, the loads considered in the virtual tests are concentrated; as a consequence, a local deformation occurs in the mesh near the load application, in a similar way as in actual experiments. Thus, local deformation effects are present in actual experiments and FEM analysis, even though there is no relationship between both effects. In both cases, experimental and numerical, all deformation effects not related to the bending and shear behaviour of the specimen are referred to as local deformation effects and are included in a stiffness term represented by a spring in the analytic approach. In the numerical case, the local deformation depends on mesh size. The model used in the analytical approach is shown in Fig. 3. Furthermore, the coordinate system, boundary conditions, loading and mesh of the FEM model are shown in Fig. 4.
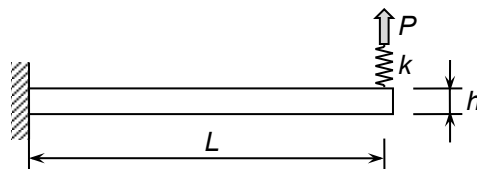

Fig. 3. Model of the three-point bending test including local deformation effects.
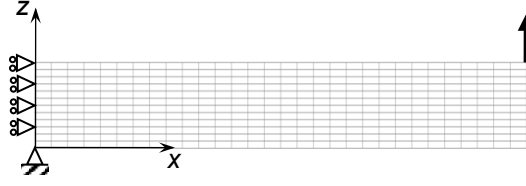
Fig. 4. Finite element model coordinate system, discretization, loading and boundary conditions.

The complementary strain energy of the cantilever beam considering bending, shear and local deformation is given by:

$$U^* = \int_L \frac{M^2}{2E_f I}dl + \frac{6}{5}\int_L \frac{Q^2}{2G_{13}A}dl + \frac{P^2}{2k} \tag{7}$$

Where M is the bending moment, Q is the shear force, P is the force at the support, E_f is the flexural modulus, G_{13} is the out-of-plane shear modulus, I is the moment of inertia, A is the cross sectional area and k is the spring constant or local deformation stiffness. The displacement δ of the loading point can be determined according to the theorem of Engesser-Castigliano [51]:

$$\delta = \frac{\partial U^*}{\partial P} = \int_L \frac{MM'}{E_f I}dl + \frac{6}{5}\int_L \frac{QQ'}{G_{13}A}dl + \frac{PP'}{k} = \frac{4PL^3}{E_f bh^3} + \frac{6}{5}\frac{PL}{G_{13}bh} + \frac{P}{k} \tag{8}$$

Rearranging terms, it results:

$$\delta = \frac{4PL^3}{E_f bh^3}\left[1 + \frac{3}{10}\frac{E_f}{G_{13}}\left(\frac{h}{L}\right)^2 + \frac{E_f b}{4k}\left(\frac{t}{L}\right)^3\right] \tag{9}$$

Eq. (9) can be written as:

$$E_f = \frac{4mL^3}{bh^3}\left[1 + \frac{3}{10}\frac{E_f}{G_{13}}\left(\frac{h}{L}\right)^2 + \frac{E_f b}{4k}\left(\frac{h}{L}\right)^3\right] \tag{10}$$

Where $m = P/\delta$ is the slope of the load-displacement curve. Terming:

$$E_0 = \frac{4mL^3}{bh^3} \tag{11}$$

Eq. (10) results:

$$E_0^{-1} = E_f^{-1} \left[1 + \frac{3}{10} \frac{E_f}{G_{13}} \left(\frac{h}{L} \right)^2 + \frac{E_f b}{4k} \left(\frac{h}{L} \right)^3 \right]$$ (12)

Eq. (12) can be written as:

$$y = A_R + B_R x^2 + C_R x^3$$ (13)

Where:

$$y = E_0^{-1}, \quad \text{x} = \frac{h}{L}, \quad A_R = E_f^{-1}, \quad B_R = \frac{3}{10} G_{13}^{-1}, \quad C_R = \frac{1}{4} \left(\frac{k}{b} \right)^{-1}$$ (14)

Once n numerical values concerning to n FEM analyses relative to different spans are obtained, the coefficients A_R, B_R and C_R in Eq. (13) can be determined using the minimum squares method as explained in [49]. After obtaining those coefficients, E_f, G_{13} and k are:

$$E_f = A_R^{-1}, \quad G_{13} = \frac{3}{10} B_R^{-1}, \quad k = \frac{b}{4} C_R^{-1}$$ (15)

It is worth pointing out that the value of the local deformation stiffness k has not been introduced in the numerical models. This value is a result of using concentrated loads in the FEM analyses, as stated above.

3. Numerical results

3.1. Flexural tests at different spans

In the numerical virtual tests a unidirectional composite of Hexcel Composites AS4-3501-6 carbon/epoxy has been considered. The mechanical properties that have been used are shown in Table 1 [54].

Table 1 Mechanical properties of the AS4-3501-6 composite

E_1 (GPa)	E_2, E_3 (GPa)	G_{12}, G_{13} (GPa)	G_{23} (GPa)	ν_{12}, ν_{13}	ν_{23}
147.0	10.3	7.0	3.7	0.27	0.54

The width of the specimens was of $b = 15$ mm. The numerical tests have been performed for specimen thicknesses of $h = 3$ mm and $h = 6$ mm and four different

spans for each thickness (L in mm): 30, 40, 60, 80. In the FEM analyses, a fixed displacement has been imposed at the load point of the cantilever beam and displacement-to-span ratio has been kept constant, being $\delta/L = 0.02$. As stated previously, in these FEM virtual tests the mechanical properties given in Table 1 have been introduced as input values.

The models have been implemented in ABAQUS software [55], considering plane strain and using two dimensional continuum elements with incompatible modes (CP4EI). These elements have been selected for their improved bending behaviour in comparison to regular displacement elements [56]. The beams have been discretized into rectangular elements that were 1 mm wide and 0.25 mm high.

The numerical output of the flexural tests has been the reaction at the load point P, for each span. With each reaction value, the slope m and the term E_0 given in Eq. (11) are known and therefore, the flexural E_f and the out-of-plane shear moduli G_{13} of the material and the local deformation coefficient k are obtained as explained in the previous section.

In the FEM simulations, the possible difference between the compressive and tensile longitudinal modulus has not been taken into account. Therefore, $E_{c1} = E_{t1} = E_1 = E_f$, namely, the longitudinal modulus E_1 shown in Table 1 is also the flexural modulus E_f.

In the case of plane strain, the flexural modulus E_f' has to be multiplied by $\left(1 - \nu_{13}\nu_{31}\right)$ in order to determine the actual modulus:

$$E_f = E_f' \left(1 - \nu_{13}\nu_{31}\right) \tag{16}$$

Fig. 5 shows the values of the flexural modulus obtained for $h = 3$ mm and $h = 6$ mm beam thicknesses.
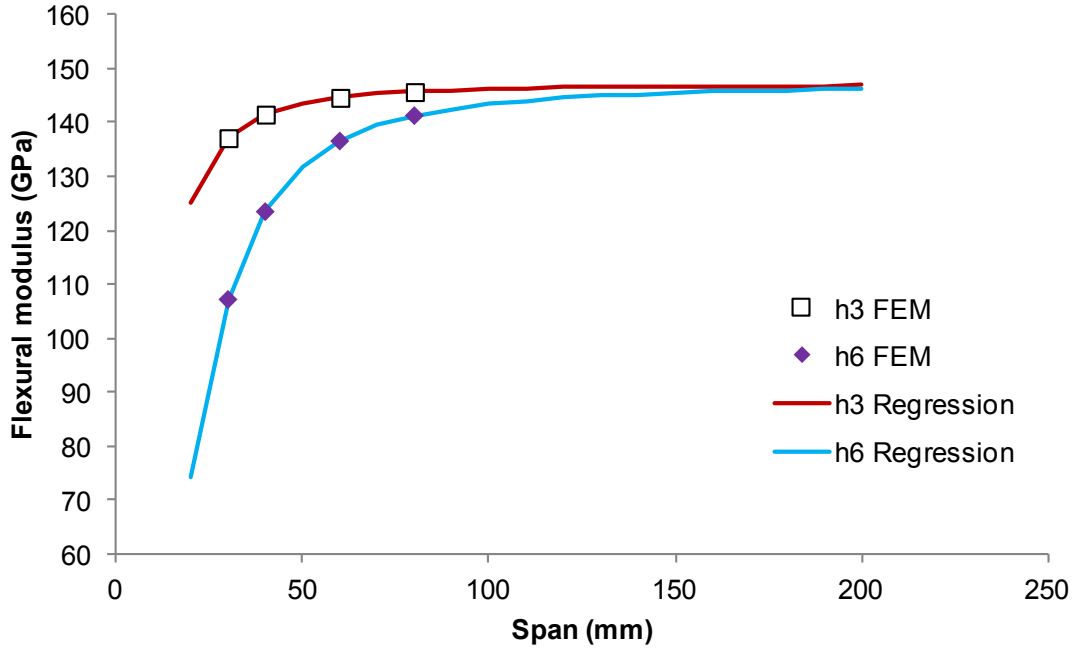
Fig. 5. Regression and FEM flexural modulus relative to $h = 3$ mm and $h = 6$ mm.

The values of the flexural E_f and the out-of-plane shear moduli G_{13} and the local deformation coefficient k obtained from the numerical analyses and relative to 3 and 6 mm thickness beams are shown in Table 2. The elastic properties obtained from FEM without taking into account k are also included. If local deformations included in the term k are considered, the results show good agreement with the input values. In contrast, if local deformations are not taken into account the errors with respect to input values are much greater: in the case of G_{13} the relative error when $h = 6$ mm increases from 4 % to 34 %; when $h = 3$ mm the relative error increases from 5 % to 13 %. Therefore, to consider the local deformation coefficient k is necessary in order to determine the elastic properties of the material via FEM.

Table 2 Flexural and out-of-plane shear moduli corresponding to $h = 3$ mm and $h = 6$ mm.

		Considering k		Without considering k	
		h (mm)		h (mm)	
	Input FEM	3	6	3	6
E_1 (MPa)	147000	147000	147000	147246	149764

12

E_3 (MPa)	10300				
G_{13} (MPa)	7000	7363	7307	6056	4593
v_{13}	0.27				
k (N/mm)		47424	34386		

3.2. Crack length

After determining E_f and G_{13}, a DCB virtual test has been carried out by FEM using ABAQUS software, as shown in Fig. 6. As in the previous FEM analyses, two dimensional continuum plane strain elements with incompatible modes have been employed. In order to include the effect of the concentrated load application, the system compliance has been obtained using FEM, applying the same loading configuration as in the DCB test to non-cracked specimens. Therefore, the compliance of the specimen is:

$$C = C_{num} - C_{sys} = \frac{2\delta}{P} - C_{sys} \tag{17}$$

In the studied cases, as the results concerning crack length are not affected by the system compliance, the correction of Eq. (17) is not necessary.
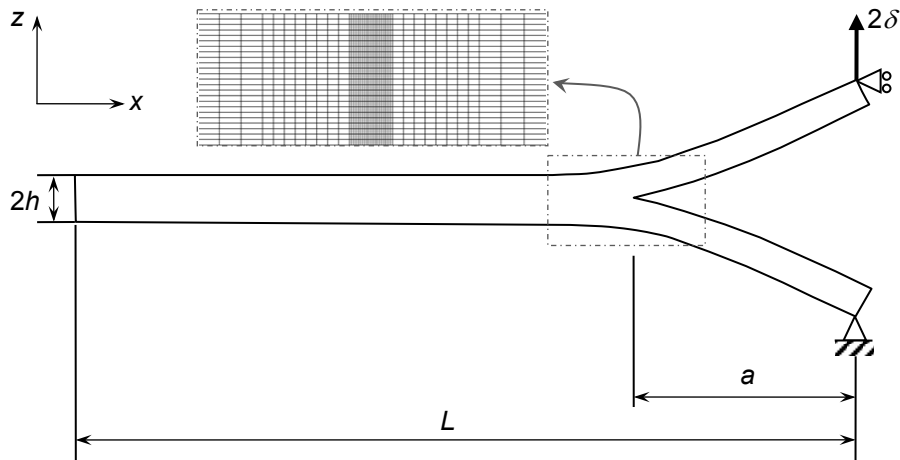

Fig. 6. Finite element model boundary conditions and detail of mesh near the crack tip.

The total length of the specimen has been L = 150 mm, the crack length a = 50 mm, the width b = 15 mm and two thickness values have been used in the numerical analyses: h = 1.5 mm and h = 3 mm. The values of E_f and G_{13} in the "Considering k" column presented in Table 2 have been used in the FEM models as input parameters. The beams have been discretized into rectangular elements, 1 mm wide and 0.25 mm high. Smaller elements have been used around the crack tip due to the stress concentration. A fixed displacement of 1 mm has been imposed.

The crack length has been calculated by means of an iterative method and for different approaches of the DCB specimen's compliance. As a first approach, the initial expression of references [9,48] has been used, which corresponds to the approximate equation of the compliance obtained from beam theory, including shear effects:

$$C = \frac{2a^3}{3E_f I} + \frac{12a}{5G_{13}A} \tag{18}$$

As a second approach, the crack length has been calculated by means of the expression for the compliance proposed in [48] that is given in Eq. (4).

The results obtained with these formulas have been compared with those achieved by means of the expressions given in references [5,6,9]. The results are shown in Table 3.

Table 3 Crack length in mm for h = 1.5 mm and h = 3.0 mm.

	a (mm)	
h (mm)	1.5	3.0
Eq. (18)	52.2	54.5
Eq. (4)	49.5	49.1
Whitney	49.7	49.5
Williams	50.2	50.5
Olsson	49.5	49.3

The results of crack length obtained using the equation proposed in [48] show good agreement with the theoretical crack length of the FEM models. These values are better in the case of small thicknesses.

3.3.   Interlaminar normal load distribution ahead of the crack tip

The analytical load distribution near the crack tip has been compared with the distribution obtained by FEM analysis in Fig. 7. The comparison has been carried out for both arm thicknesses: $h = 1.5$ mm and $h = 3.0$ mm for the displacement that corresponds to the critical value of the energy release rate.
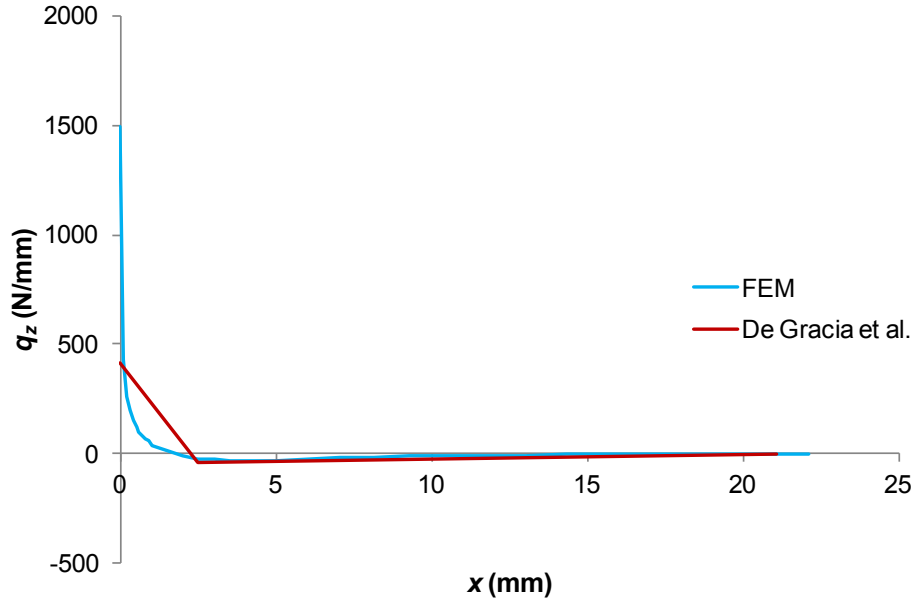
(a)

(b)
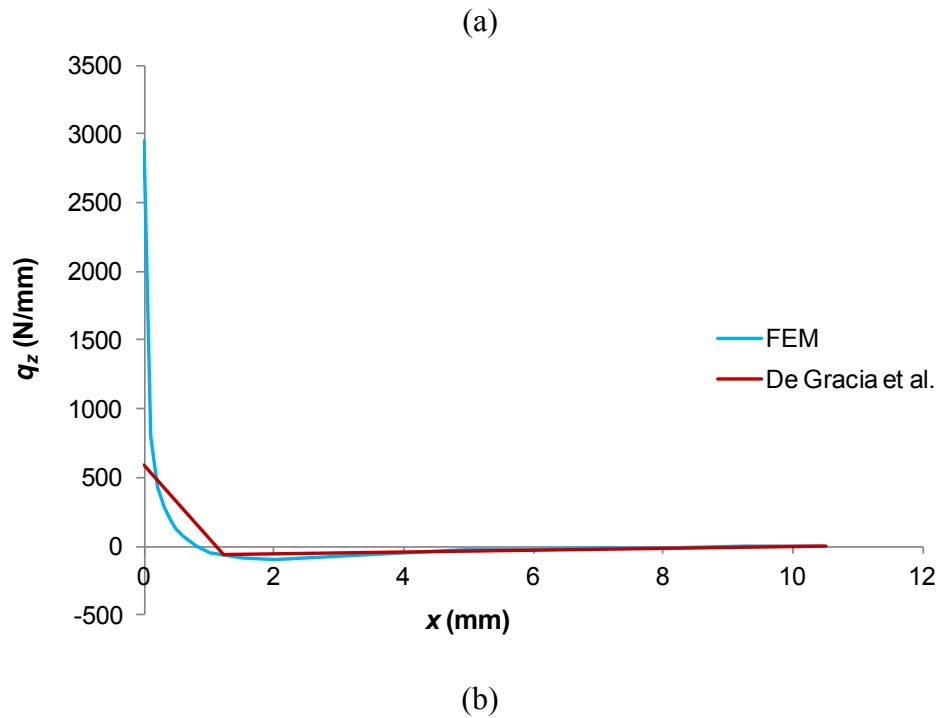
Fig. 7. Comparison of the analytical and numerical load distributions; a) $h = 1.5$ mm; b) $h = 3.0$ mm.

The areas of tensile and compressive sides determined analytically and numerically agree in both cases. Furthermore, the length of both distributions also agree, increasing when the thickness increases.

3.4. Energy release rate

In this section the energy release rate G_I has been calculated analytically and numerically.

According to Coronado et al. [21], the critical strain energy release rate G_{Ic} of AS4-3501-6 carbon/epoxy unidirectional composite is $G_{Ic} = 130$ J/m². With this value the maximum load P_c can be estimated by Eq. (6). The displacement at the loading point is obtained from Eq. (4) being $2\delta = 3.24$ mm when $h = 1.5$ mm and $2\delta = 1.25$ mm when $h = 3$ mm. Taking into account Eq. (5) and Eq. (18) and replacing P_c, E_f, G_{13} and $a = 50$ mm, G_{Ic} is determined from beam theory with shear effects. Replacing in Eq. (6) P_c, E_f and G_{13} of Table 2 and the crack length shown in Table 3, G_{Ic} is determined from the analytical approach.

The displacements obtained previously have been imposed in the FEM model. The energy release rate G_{Ic} is given by [57]:

16

$$G_{Ic} = -\frac{1}{b}\left(\frac{\partial U}{\partial a}\right)_{\delta} \qquad (19)$$

Where U is the total strain energy, b is the width, a is the crack length and δ means that constant displacement conditions apply.

G_{Ic} can be obtained numerically by different methods: taking into account the strain energy change for a small crack advance Δa and applying Eq. (19); by VCCT method [25]; using the Two-step extension method (TSEM) [58] and applying the area method. Those methods have been applied in the numerical model and as the results obtained are the same for the precision used, only one column of FEM results has been included in Table 4.

The energy release rate has been determined for three different increases in delamination length Δa. The analytical and numerical results of G_{Ic} are shown in Table 4. The analytical values obtained from Eq. (6) [48] are in good agreement with numerical results. Otherwise, the values of G_{Ic} determined using beam theory with shear effects, using Eq. (5) and Eq. (18), differ significantly from those obtained from Eq. (6) and from FEM analyses, as this approach does not include crack tip rotation.

Table 4 Analytical and numerical critical strain energy release rate in J/m².

G_{Ic} (J/m²)	Analytical expressions		FEM
	Beam theory	De Gracia et al.	
$h = 1.5$ mm			
$\Delta a = 0.1$ mm	119.1	130.3	129.3
$\Delta a = 0.2$ mm	119.3	130.4	129.0
$\Delta a = 0.5$ mm	119.8	130.8	128.1
$h = 3.0$ mm			
$\Delta a = 0.1$ mm	107.8	128.8	127.7
$\Delta a = 0.2$ mm	108.0	129.0	127.4
$\Delta a = 0.5$ mm	108.5	129.4	126.6

4. Conclusions

This study deals with the numerical assessment of an experimental procedure used to reduce data in DCB tests. Two main conclusions can be inferred:

- If the virtual three-point bending tests at different spans are carried out taking into account local deformation effects, the flexural and shear moduli of the material obtained after data reduction show good agreement with the input values. On the contrary, when local deformations are not considered the errors with respect to input values are significantly greater. Therefore, to determine the flexural and shear moduli from finite element analysis, it is necessary to include the local deformation effects.

- The results obtained for the crack length, the load distribution and the critical energy release rate from DCB virtual tests are in good agreement with those analytical. Thus, the experimental procedure introduced by De Gracia et al. based on an analytic approach has been validated numerically.

References

[1] ISO. "15024, Fiber-reinforced plastic composites - determination of mode I interlaminar fracture toughness, GIC, for unidirectionally reinforced materials". 2001.

[2] ASTM. "Standard D5528-13, Standard Test Method for Mode I Interlaminar Fracture Toughness of Unidirectional Fiber-Reinforced Polymer Matrix Composites". ASTM International, West Conshohocken, PA, 2013, www.astm.org.

[3] Kanninen MF. An augmented double cantilever beam model for studying crack propagation and arrest. Int J Fract 1973;9:83-92.

[4] Kanninen MF. A dynamic analysis of unstable crack propagation and arrest in the DCB test specimen. Int J Fract 1974;10:415-30.

[5] Whitney JM. Stress analysis of the double cantilever beam specimen. Compos Sci Technol 1985;23:201-19.

[6] Williams JG. End corrections for orthotropic DCB specimens. Compos Sci Technol 1989;35:367-76.

[7] Hashemi S, Kinloch AJ, Williams JG. Corrections needed in double-cantilever beam tests for assessing the interlaminar failure of fibre-composites. J Mater Sci Lett 1989;8:125-9.

[8] Williams JG. Large Displacement and End Block Effects in the 'DCB' Interlaminar Test in Modes I and II. J Compos Mater 1987;21:330-47.

[9] Olsson R. A simplified improved beam analysis of the DCB specimen. Compos Sci Technol 1992;43:329-38.

[10] Kondo K. Analysis of double cantilever beam specimen. Adv Compos Mater 1995;4:355-66.

[11] Nageswara Rao B, Acharya AR. Evaluation of fracture energy GIC using a double cantilever beam fibre composite specimen. Eng Fract Mech 1995;51:317-22.

[12] Ozdil F, Carlsson LA. Beam analysis of angle-ply laminate DCB specimens. Compos Sci Technol 1999;59:305-15.

[13] Bruno D, Greco F. Mixed mode delamination in plates: a refined approach. Int J Solids Struct 2001;38:9149-77.

[14] Yoshihara H, Kawamura T. Mode I fracture toughness estimation of wood by DCB test. Compos Part A-Appl S 2006;37:2105-13.

[15] Hamed MA, Nosier A, Farrahi GH. Separation of delamination modes in composite beams with symmetric delaminations. Mater Design 2006;27:900-10.

[16] Gunderson JD, Brueck JF, Paris AJ. Alternative test method for interlaminar fracture toughness of composites. Int J Fract 2007;143:273-6.

[17] Pavan Kumar DVTG, Raghu Prasad BK. Analysis of unidirectional (0°) fiber-reinforced laminated composite double cantilever beam specimen using higher order beam theories. Eng Fract Mech 2008;75:2156-74.

[18] Shokrieh MM, Heidari-Rarani M, Ayatollahi MR. Interlaminar fracture toughness of unidirectional DCB specimens: A novel theoretical approach. Polym Test 2012;31:68-75.

[19] Franklin VA, Christopher T. Fracture Energy Estimation of DCB Specimens Made of Glass/Epoxy: An Experimental Study. Adv Mater Sci Eng 2013:412601.

[20] Szekrényes A, Uj J. Advanced beam model for fiber-bridging in unidirectional composite double-cantilever beam specimens. Eng Fract Mech 2005;72:2686-702.

[21] Coronado P, Argüelles A, Viña J, Mollón V, Viña I. Influence of temperature on a carbon–fibre epoxy composite subjected to static and fatigue loading under mode-I delamination. Int J Solids Struct 2012;49:2934-40.

[22] Coronado P, Argüelles A, Viña J, Bonhomme J, Mollón V. Influence on the delamination phenomenon of matrix type and thermal variations in unidirectional carbon-fiber epoxy composites. Polym Compos 2014;36:747-55.

[23] Argüelles A, Viña J, Canteli AF, Coronado P, Mollón V. Influence of temperature on the delamination process under mode I fracture and dynamic loading of two carbon–epoxy composites. Compos Part B-Eng 2015;68:207-14.

[24] Shokrieh MM, Heidari-Rarani M. A comparative study for beams on elastic foundation models to analysis of mode-I delamination in DCB specimens. Struct Eng Mech 2011;37:149-62.

[25] Rybicki EF, Kanninen MF. A finite element calculation of stress intensity factors by a modified crack closure integral. Eng Fract Mech 1977;9:931-8.

[26] Bennati S, Colleluori M, Corigliano D, Valvo PS. An enhanced beam-theory model of the asymmetric double cantilever beam (ADCB) test for composite laminates. Compos Sci Technol 2009;69:1735-45.

[27] Mollón V, Bonhomme J, Viña J, Argüelles A. Mixed mode fracture toughness: An empirical formulation for GI/GII determination in asymmetric DCB specimens. Eng Struct 2010;32:3699-703.

[28] Shokrieh MM, Heidari-Rarani M, Rahimi S. Influence of curved delamination front on toughness of multidirectional DCB specimens. Compos Struct 2012;94:1359-65.

[29] Shokrieh MM, Zeinedini A. A Novel Method for Calculation of Strain Energy Release Rate of Asymmetric Double Cantilever Laminated Composite Beams. Appl Compos Mater 2014;21:399-415.

[30] Valvo PS. A revised virtual crack closure technique for physically consistent fracture mode partitioning. Int J Fract 2012;173:1-20.

[31] Valvo PS. A further step towards a physically consistent virtual crack closure technique. Int J Fract 2015;192:235-44.

[32] Kravchenko OG, Kravchenko SG, Sun C. Thickness dependence of mode I interlaminar fracture toughness in a carbon fiber thermosetting composite. Compos Struct 2017;160:538-46.

[33] Szekrényes A, Uj J. Comparison of some improved solutions for mixed-mode composite delamination coupons. Compos Struct 2006;72:321-9.

[34] Szekrényes A. Improved analysis of unidirectional composite delamination specimens. Mech Mater 2007;39:953-74.

[35] Szekrényes A. Semi-layerwise analysis of laminated plates with nonsingular delamination—The theorem of autocontinuity. Appl Math Model 2016;40:1344-71.

[36] Szekrényes A. Nonsingular crack modelling in orthotropic plates by four equivalent single layers. Eur J Mech A-Solid 2016;55:73-99.

[37] Turon A, Dávila CG, Camanho PP, Costa J. An engineering solution for mesh size effects in the simulation of delamination using cohesive zone models. Eng Fract Mech 2007;74:1665-82.

[38] de Moura MFSF, Campilho RDSG, Gonçalves JPM. Crack equivalent concept applied to the fracture characterization of bonded joints under pure mode I loading. Compos Sci Technol 2008;68:2224-30.

[39] de Moura MFSF, Morais JJL, Dourado N. A new data reduction scheme for mode I wood fracture characterization using the double cantilever beam test. Eng Fract Mech 2008;75:3852-65.

[40] de Moura MFSF, Campilho RDSG, Amaro AM, Reis PNB. Interlaminar and intralaminar fracture characterization of composites under mode I loading. Compos Struct 2010;92:144-9.

[41] Morais JJL, de Moura MFSF, Pereira FAM, Xavier J, Dourado N, Dias MIR et al. The double cantilever beam test applied to mode I fracture characterization of cortical bone tissue. J Mech Behav Biomed 2010;3:446-53.

[42] Sebaey TA, Blanco N, Lopes CS, Costa J. Numerical investigation to prevent crack jumping in Double Cantilever Beam tests of multidirectional composite laminates. Compos Sci Technol 2011;71:1587-92.

[43] de Morais AB. Mode I cohesive zone model for delamination in composite beams. Eng Fract Mech 2013;109:236-45.

[44] Mollón V, Bonhomme J, Elmarakbi AM, Argüelles A, Viña J. Finite element modelling of mode I delamination specimens by means of implicit and explicit solvers. Polym Test 2012;31:404-10.

[45] Huang D, Sheng B, Shen Y, Chui Y. An analytical solution for double cantilever beam based on elastic–plastic bilinear cohesive law: Analysis for mode I fracture of fibrous composites. Eng Fract Mech 2018;193:66-76.

[46] Shahani AR, Abolfathitabar R. Fracture analysis of finite length angle-ply composite double cantilever beam specimens. Proc Inst Mech Eng Part C 2019;233:967-76.

[47] Xu W, Guo ZZ. A simple method for determining the mode I interlaminar fracture toughness of composite without measuring the growing crack length. Eng Fract Mech 2018;191:476-85.

[48] De Gracia J, Boyano A, Arrese A, Mujika F. A new approach for determining the R-curve in DCB tests without optical measurements. Eng Fract Mech 2015;135:274-85.

[49] Mujika F. On the effect of shear and local deformation in three-point bending tests. Polym Test 2007;26:869-77.

[50] Arrese A, Carbajal N, Vargas G, Mujika F. A new method for determining mode II R-curve by the End-Notched Flexure test. Eng Fract Mech 2010;77:51-70.

[51] Oden JT, Ripperger EA. Mechanics of Elastic Structures. 2nd ed. Washington: Hemisphere Publishing Corporation, 1981.

[52] Arrese A, Boyano A, De Gracia J, Mujika F. A novel procedure to determine the cohesive law in DCB tests. Compos Sci Technol 2017;152:76-84.

[53] Irwin GR, Kies JA. Critical energy rate analysis of fracture strength. Weld Res Suppl 1954;33:193-8.

[54] Daniel IM, Ishai O. Engineering mechanics of composite materials. Oxford University Press, 2006.

[55] Dassault Systèmes Simulia Corp. Commercial software ABAQUS Standard, version 6.12. 2012.

[56] Dassault Systèmes Simulia Corp. ABAQUS Theory Manual, 6.12. 2012.

[57] Boyano A, Mollón V, Bonhomme J, De Gracia J, Arrese A, Mujika F. Analytical and numerical approach of an End Notched Flexure test configuration with an inserted roller for promoting mixed mode I/II. Eng Fract Mech 2015;143:63-79.

[58] Bonhomme J, Argüelles A, Castrillo MA, Viña J. Computational models for mode I composite fracture failure: the virtual crack closure technique versus the two-step extension method. Meccanica 2010;45:297-304.